

PMSM Parameter Estimation for Sensorless FOC Based on Differential Power Factor

Carlos Candelo-Zuluaga, Jordi-Roger Riba, and Antoni Garcia

Abstract— During the last years, different methods for identifying permanent magnet synchronous motor (PMSM) parameters have been developed. Such methods allow a better characterization of PMSMs thus enabling a better control. This paper presents a novel PMSM parameter estimation method based on the differential power factor due to the harmonic distortion, which allows the identification of the motor parameters from data acquisitions representing the entire torque-speed range. This method does not require measuring any geometric parameters, thus avoiding motor disassembly, or prior knowledge of the applied field oriented control (FOC) strategy. It also enables identifying the current, voltage and d - q components of the flux linkage without knowing the rotor position. The proposed method is based on a d - q electrical model that considers the harmonic components of the electrical magnitudes. It avoids to apply any optimization technique, thus requiring a low computational burden. The method is first validated experimentally by comparing the identified d - q current space vector against the acquired one using a resolver associated with a commercial drive. Finally, it is further validated by using a second PMSM associated to a sensorless drive, comparing the identified d - q inductances with ground truth data obtained by a validated method.

Index Terms— Permanent magnet machines, parameter estimation, field oriented control, performance analysis, performance evaluation, system identification.

NOMENCLATURE

A_{DAQ}	DAQ accuracy [V]
A_t	Total measurement accuracy [V]
A_{Trans}	Transducer accuracy [V]
$\cos(\varphi)$	Power factor [-]
E_{pm-1st}	1 st Harmonic permanent magnet stator back-electromotive force [V]
E_s	Stator back-electromotive force [V]
I_{abc}	Stator phase currents [A]
i_d	Direct axis current [A]
i_q	Quadrature axis current [A]
i_s	Current space vector [A]
i_{s-nth}	n -th harmonic of the current space vector [A]
I_s	Rated stator current [A]
L_d	Direct axis inductance [H]
L_q	Quadrature axis inductance [H]
m	Phases number [-]
n	Rotor angular speed [rpm]
n_{max}	Maximum rotor angular speed [rpm]
p	Pairs of poles [-]

P_{Fe-mec}	Iron and mechanical losses sum [W]
P_{Rs}	Copper losses [W]
P_U	Useful mechanical power [W]
q	Number of slots per pole and phase [-]
R_{Fe}	Iron resistance [Ω]
R_s	Stator windings per phase resistance [Ω]
R_{so}	Phase stator resistance at ambient temperature [Ω]
T	Output mechanical torque [N·m]
T_{amb}	Ambient temperature [$^{\circ}$ C]
T_{wl}	Winding temperature (front coil head) [$^{\circ}$ C]
T_{w2}	Winding temperature (rear coil head) [$^{\circ}$ C]
U_{abc}	Stator phase voltages [V]
u_d	Direct stator voltage [V]
u_q	Quadrature stator voltage [V]
u_s	Voltage space vector [V]
u_{s-nth}	n -th harmonic of the stator voltage space vector [V]
$u(x_i)$	Standard uncertainty
$u_c(y)$	Combined standard uncertainty
$u^2(x_i)$	Estimated variance
$u_c^2(y)$	Combined estimated variance
U_{dc}	Voltage of the DC bus [V]
U_s	Rated stator voltage [V]
α	Angle between the 1 st harmonic of the stator flux linkage and the current [rad]
β	Angle between the 1 st harmonic of the stator voltage and the back-electromotive force
η	Energy efficiency [p.u.]
θ_e	Electrical angular position [rad]
θ_{is-1st}	First harmonic current space vector angle [rad]
θ_m	Mechanical angular position [rad]
θ_{res}	Resolver angular position [rad]
θ_{us-1st}	First harmonic voltage space vector angle [rad]
φ	First harmonic power factor angle [rad]
ω_m	Electrical angular speed [rad/s]
Ψ_{abc}	Stator flux linkage [V·s/rad]
Ψ_d	Direct axis flux linkage [V·s/rad]
Ψ_{pm}	Permanent magnets flux linkage [V·s/rad]
Ψ_{pm-1st}	1 st harmonic permanent magnets flux linkage [V·s/rad]
Ψ_q	Quadrature axis flux linkage [V·s/rad]
Ψ_{s-1st}	1 st harmonic stator flux linkage [V·s/rad]

I. INTRODUCTION

PARAMETER estimation for electrical machines is an active research topic which enables characterizing the operational performance and to improve the behavior of whole PMSM drive systems [1]. PMSMs require special attention among other electrical machines due to their superior capabilities, such

The authors would like to thank the support of the Generalitat de Catalunya under the Industrial Doctorate 2018 DI 004 and 2017SGR0967 projects, as well as the Spanish Ministry of Economy and Competitiveness under the project TRA2016-80472-R.

Carlos Candelo-Zuluaga, Jordi-Roger Riba and Antoni Garcia are with the Electrical Engineering Department, Universitat Politècnica de Catalunya, Barcelona 08034, Spain (e-mail: carlos.andres.candelo@upc.edu; jordi.riba-ruiz@upc.edu; antoni.garcia@upc.edu).

as high torque density, high precision, high dynamic performance adaptability, or reduced power loss among other relevant features [2]. To take advantage these characteristics, it is necessary to apply advanced vector control algorithms, most of them without using position sensors [3]. The accurate identification of the motor parameters improves and optimizes the use of PMSM drives. Finite element analysis (FEA) is commonly used to extract the PMSM parameters [4], because it allows computing motor performance by considering different load and temperature conditions. Nevertheless, apart from the intensive computational burden, FEA requires a deep knowledge of the motor geometry, winding topology and materials. It increases the difficulty to characterize the PMSM because manufacturers usually do not provide all data required to build an accurate model. Therefore, the most suitable way for parameter identification is to apply algorithms that only require measurable data, such as voltages, currents or rotor speed [5]. Different methods can be applied to this end, which are divided into two categories, i.e., online and offline identification [6]. An early study [7] presents an experimental approach for identifying the magnetic model parameters of different types of synchronous machines by evaluating the flux linkages from the voltage acquisitions. Some variants were introduced in [8], where the magnetic model is identified exclusively by test, thus do not requiring an offline mathematical manipulation. Some improvements are found in [9], where cross-saturation and magnetic saturation effects are considered at standstill, with or without the need to lock the rotor. Other studies focus on finding the rotor position by analyzing the current waveforms [10] in direct current or switched reluctance machines without using a position sensor [11].

Online parameter identification is focused to identify the PMSM parameters during real-time operation. Therefore, it is not necessary to stop the motor if the data measured by the transducers is already accessible. Online parameter identification methods fall into three categories, i.e., numerical methods [12]–[14], observer-based methods [15]–[18] and artificial intelligence (AI)-based methods [1][19]. In [20] the disturbance voltage influence on the accuracy of the estimation is analyzed, whereas [21] proposes an online sensorless speed tracking for PMSMs. In [22] an active flux based sensorless control to provide rotor position estimation at low-speed regimes is evaluated. Some other improvements were presented in [23], allowing to identify the stator resistance and permanent magnet flux linkage of three-phase, open-end winding PMSMs. More recent studies focus on specific features of sensorless controls. For instance, [24] presents an on-line identification method to detect the load current at low speed regimes, which is affected by the position estimation error. In [25], an online parameter identification based on a high frequency (HF) equivalent impedance model is presented, allowing the use of the method either online or offline. Off-line methods are designed to obtain the data in advance for further parameter estimation. They require stopping the motor operation and performing different experiments to extract the data. There are three different categories of off-line methods, i.e., frequency domain methods [26], [27], time domain methods [5], [28] and finite element methods [29].

This paper presents a novel PMSM parameter estimation method. First, the method characterizes the motor parameters

by considering its performance on the entire torque-speed range, thus, allowing to find the parameter variations as a function of the load conditions. Moreover, as a main novelty, the identification method finds the values of the d - q inductances from the differential power factor due to the harmonic distortion. This method calculates the d - q inductances as a function of the space vector current and angle, thus providing superior accuracy compared to most of the approaches found in the literature. The proposed method finds the vectors magnitudes and angle without requiring any position sensor, motor geometry information or prior knowledge of the applied FOC strategy. This approach uses a d - q electrical model considering the harmonics of the electrical magnitudes, and does not apply any optimization algorithm for the identification, thus reducing computational requirements. It is worth noting that by considering the harmonics, the d - q inductances are characterized more accurately and realistically, thus allowing an enhanced characterization of the machine and to apply improved control strategies.

This paper also contributes in the field of instrumentation and measurement as it proposes a method that from electrical and mechanical measurements (voltages, currents, torque and speed), the d - q inductances of PMSMs are inferred in the entire torque-speed map as a function of the operating point. These parameters are usually obtained by means of FEM models, so they are not directly measured. In case of being measured, a test bench equipped with an accurate position sensor on the motor shaft is required, thus carrying out a set of tests for each rotor angular position. The method presented in this paper avoids the need for such a position sensor.

As the main objective is to identify the PMSM parameters in the whole torque-speed range, the method can be classified as off-line. Nevertheless, it can be used on-line, as well as for identifying the electromagnetic parameters using a single operating point. The proposed method is first validated experimentally by comparing the identified d - q current space vector against that acquired by using the position provided by a resolver connected to an ABB DGV700 converter that applies a 90° current control without flux weakening capability. The method is further validated by using a second PMSM connected to a Renessa's YROTATE-IT-RX23T motor control platform, which applies a sensorless 90° current control with flux weakening capability. The d - q inductances are validated for all experimental operational points.

II. PMSM PARAMETER ESTIMATION METHODOLOGY OVERVIEW

This section introduces the parameter estimation methodology, detailing the data required, the different applied tests, and the output data. Fig. 1 shows the process diagram divided in two main stages, i.e., the experimental tests and the parameter estimation stage.

The parameters to be known beforehand are the rated magnitudes, including the line voltage, phase current, rated and maximum speed, rated torque, number of phases and number of poles, which are usually found in the motor nameplate. Next, some optional tests can be performed to obtain the permanent magnet flux linkage and phase resistance. These values will be taken as seed values for the solution, although they will be corrected when identifying the PMSM parameters. Then, the

motor is tested for the whole torque-speed range, acquiring for each tested operating point the phase currents, line voltages, load torque, angular speed, resolver or encoder position (just to validate the methodology) and the winding temperature. This time-varying information is acquired during the experiments. Finally, the parameter estimation algorithm is applied to identify the FOC strategy and the electromagnetic parameters over the whole torque-speed range.

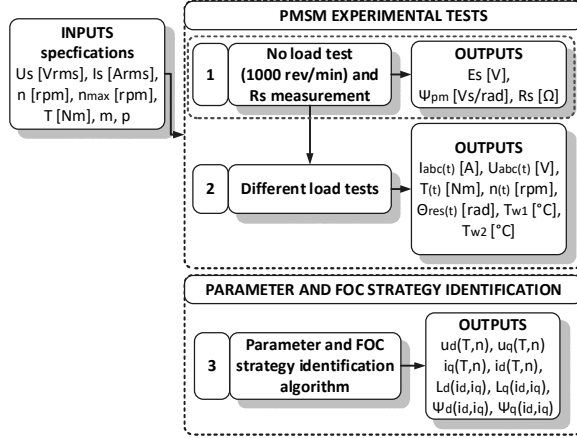


Fig. 1. PMSM parameter estimation methodology

III. PMSM TESTING METHODOLOGY

This section details the experimental procedure followed to extract the data. Fig. 2 summarizes the PMSM testing process.

As already mentioned, the input data are usually available in the motor nameplate. Nevertheless, some other parameters can be obtained and updated to their current values, because they can change for different reasons such as tolerances in the manufacturing process, aging or faults among others.

A. PMSM no load test

First, the no load test (steps 1 and 2) is performed at 1000 rpm to acquire the time dependent back-electromotive force due to the permanent magnets, while extracting the harmonic components of the permanent magnet flux linkage. The winding resistance is also measured at ambient temperature. These data are used as seed values, being updated during the estimation process.

B. PMSM load tests

Next, the motor is connected to the load motor as shown in Fig. 3. The load test consists in evaluating different operating points within the torque-speed plane (steps 3 to 7).

1) Torque-speed discretization

To test the motor along the entire torque-speed range, it is discretized considering the rated torque and the rated and maximum angular speeds. The maximum power envelope is considered as a limit to set the maximum speed for each torque value.

2) Operating point test and data acquisition

Once the torque-speed map is discretized, time-dependent data measurements are acquired for all operating points. These data include the phase currents, line voltages, dynamic torque, dynamic angular speed, motor resolver position and winding temperature. In case of having a position sensor, the measured

rotor position is used to validate the accuracy of the identified current space vector angle.

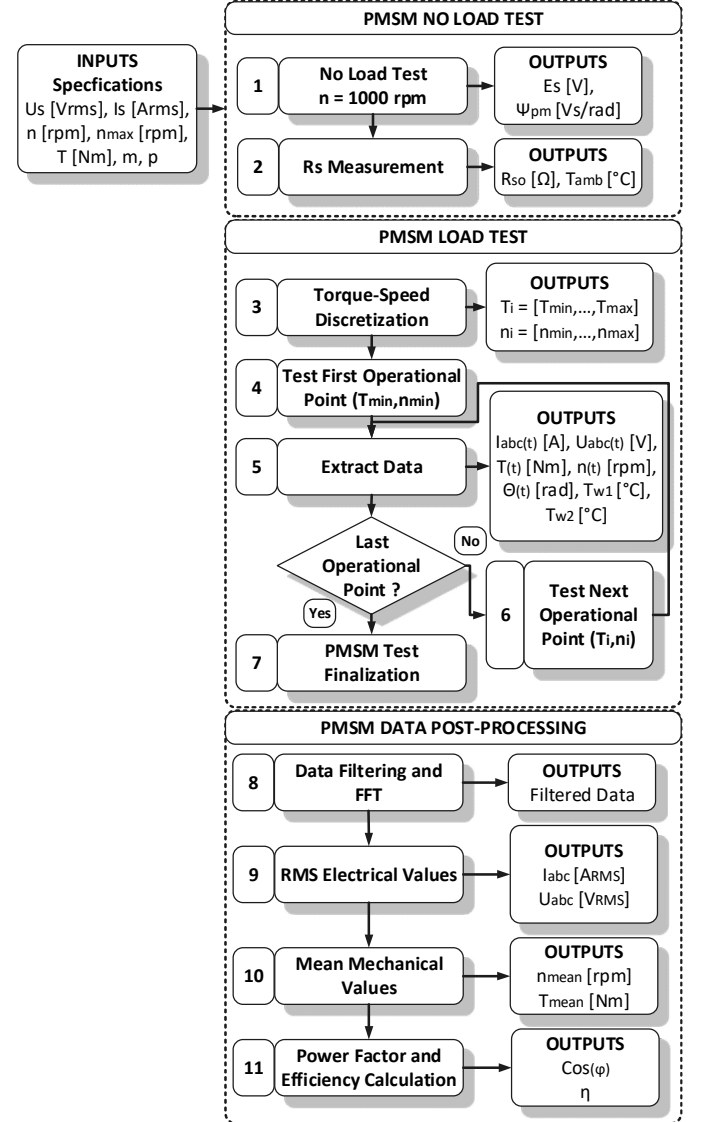


Fig. 2. PMSM test process

Table I shows the details of the measurement and acquisition of the acquired magnitudes.

TABLE I
MEASUREMENT AND ACQUISITION DETAILS

Magnitude	Sampling Frequency	Number of samples	DAQ Input Range	DAQ Sensitivity	DAQ Accuracy	Transducer Accuracy
Angular speed sensor	200 kS/s	200 kS	±5 V	56 μV	1.01 mV	0.15 V
Current sensors			±1 V	12.8 μV	0.22 mV	5 mV
Torque sensor			±10 V	112 μV	1.92 mV	0.02 V
Voltage sensors			±5 V	56 μV	1.01 mV	3 mV
Temperature sensors	1 S/s	1 S	±1 V	12.8 μV	0.22 mV	88 μV

C. PMSM data processing

Finally, the data is post-processed (steps 8 to 11). This stage include different steps which are described below.

1) Data filtering and calculations

As indicated in Table I, the signals are acquired at a sampling frequency of 200 kS/s for 1 second for each operational point. The PMSMs tested in this study have six pole extensions, with a maximum angular speed of 6000 rpm, so the maximum fundamental is 300 Hz, corresponding to 66 samples per period. Assuming a minimum of 8 samples per period to properly acquire a sinusoidal signal, this system allows acquiring up to the 83th harmonic. The data is filtered by applying a first-order low-pass filter with a stopband attenuation of 60 dB. The cut-off frequency is set to the frequency of the 7th electrical harmonic, the highest relevant harmonic for a proper operation.

2) Fast Fourier Transformation (FFT)

After acquiring and filtering the data, a harmonic analysis is performed to extract the amplitude and phase of the fundamental, third and fifth harmonics. These values are used to identify the PMSM parameters. Finally, once all data are conditioned, the RMS values of the electrical variables and the mean values of the mechanical variables are calculated jointly with the power factor and efficiency for all operational points.

D. Experimental setup

Fig. 3 details the experimental setup used to analyze the PMSM operating points in the whole torque-speed plane and the instrumentation used.

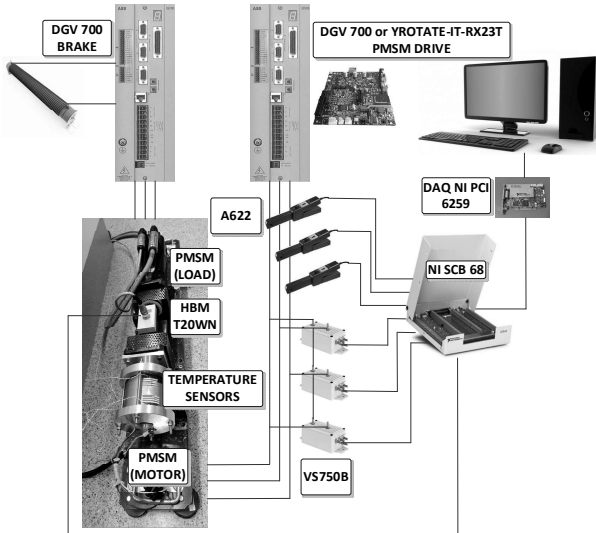


Fig. 3. Setup required to test the PMSM

Table II summarizes the instrumentation used in the experimental part.

TABLE II
INSTRUMENTATION

Converter	ABB - DGV 700 / YROTATE-IT-RX23T
Angular speed sensor	ABB-DGV700 (A I/O: $\pm 15V$, 1%)
Current sensors	Tektronix A622 (10 mV/A o 100 mV/A, sensitivity: 0.06 mV/A)
Torque sensor	HBM T20WN/20NM (Torque: 0-10 V, ± 0.2 %)
Voltage sensors	ABB VS750B (750 V, 0.3-0.9 %)
Temperature sensors	Type K Thermocouple, (0.75 %)
Data acquisition device	DAQ NI PCI-6259 - NI SCB 68 ($\pm 5V$, 56 μ V), 16 bits
Acquisition software	Python

E. Standard uncertainty and combined standard uncertainty analysis

This subsection details the standard uncertainty analysis including the DAQ and measurement devices, as well as the combined standard uncertainty for the estimated values. The accuracy of each transducer is overlapped with the accuracy of the DAQ. Fig. 4 shows the full accuracy region considering the DAQ and transducer.

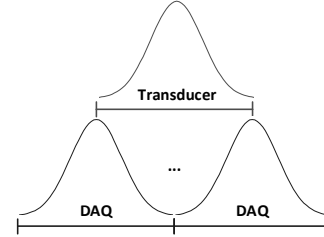


Fig. 4. DAQ and transducer accuracy disposition.

Considering the worst case scenario, the total accuracy is the sum of accuracies.

$$A_t = A_{trans} + A_{DAQ} \quad (1)$$

Assuming a coverage factor of 3, the standard uncertainty is calculated as,

$$u(x_i) = \frac{A}{3} \quad (2)$$

The estimated variance is as,

$$u^2(x_i) = (u(x_i))^2 \quad (3)$$

The combined variance of a function of interest is defined as,

$$u_c^2(y) = \sum_{i=1}^N \left[\frac{\partial f}{\partial x_i} \right]^2 \cdot u^2(x_i) \quad (4)$$

Therefore the combined standard uncertainty is used to calculate the accuracy of estimated values, which is the square root of the combined variance,

$$u_c(y) = \sqrt{u_c^2(y)} \quad (5)$$

Table III shows the standard uncertainty for measured magnitudes.

TABLE III
STANDARD UNCERTAINTY FOR MEASURED MAGNITUDES

Magnitude	DAQ Accuracy	Transducer Accuracy	Total Accuracy	Standard Uncertainty (Acquisition magnitude)	Standard Uncertainty (Physical magnitude)
Angular speed sensor	1.01 mV	0.15 V	151 mV	50.30 mV	20.12 rpm
Current sensors	0.22 mV	5 mV	5.22 mV	1.74 mV	0.0087 A
Torque sensor	1.92 mV	0.02 V	21.9 mV	7.30 mV	0.0146 Nm
Voltage sensors	1.01 mV	3 mV	3.01 mV	1.003 mV	0.15 V
Temperature sensors	0.22 mV	88 μ V	0.31 mV	0.103 mV	0.18 $^{\circ}$ C

IV. PARAMETER AND FOC STRATEGY IDENTIFICATION ALGORITHM

This section details the parameter and FOC strategy identification procedures.

A. Space vector current discretization and harmonic decomposition

First, the current space vector angle is discretized, as the aim of the algorithm is to determine the applied FOC strategy. This discretization is performed within the second quadrant because the machine to identify is a PMSM. Based on this discretization and the available data, it is possible to extract the magnitudes required to identify the control strategy for all operating points.

Fig. 5 shows a generalized d - q vector diagram of the PMSM. First, the harmonic components of the electrical magnitudes (voltage and current) are determined for all operational points. The fundamental frequency, amplitudes and phase angles of the harmonic components are obtained. The third and fifth harmonics are used for an accurate identification of the inductances for all operating points.

Fig. 6 shows the third and fifth current harmonic vector diagram, showing the areas where the current magnitude can change. Therefore, when identifying the d - q current, it is necessary to decouple the harmonic components and its effect in the voltage and flux linkage vectors.

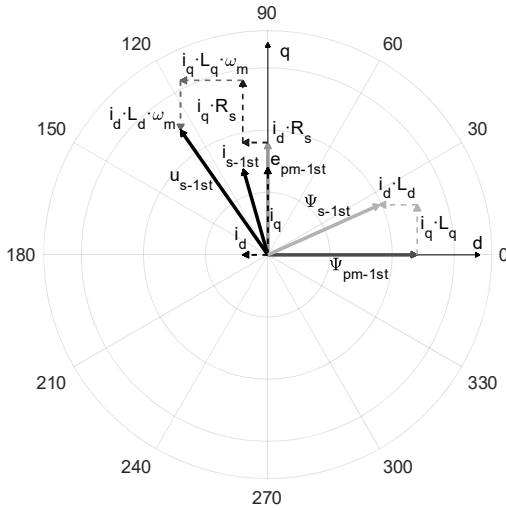


Fig. 5. Generic PMSM vector diagram of the fundamental magnitudes.

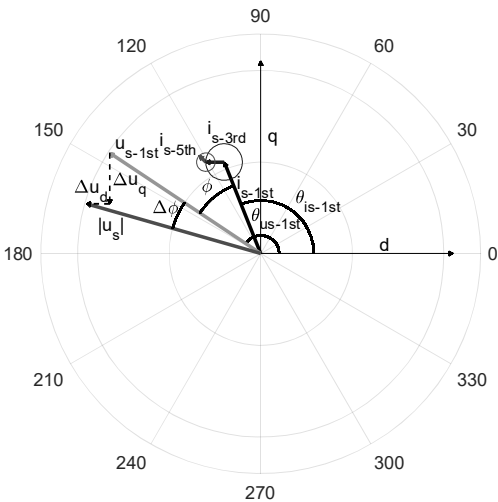


Fig. 6. Generic PMSM vector diagram including the harmonic vector representation.

B. Winding resistance adjustment, iron resistance and stator flux linkage calculation

Once the fundamental electrical magnitudes are known, the winding resistance is corrected according to its temperature,

$$R_s = R_{s_0} \cdot [1 + \alpha_{Cu} \cdot (T_w - T_{amb})] \quad (6)$$

Power losses due to the stator resistance, considering the contribution of the third and fifth harmonic current are calculated as,

$$P_{R_s} = \frac{m}{2} \cdot (i_{s-1st}^2 + i_{s-3rd}^2 + i_{s-5th}^2) \cdot R_s \quad (7)$$

From the power balance it is possible to determine the iron and mechanical power losses in all operational points.

$$P_{Fe-mec} = \left(\frac{P_U}{\eta} - P_U - P_{R_s} \right) \quad (8)$$

Assuming that the iron and mechanical losses can be represented as a parallel resistance in the d - q electrical model, R_{Fe-mec} is calculated as,

$$R_{Fe-mec} = \frac{m}{2 \cdot P_{Fe-mec}} \cdot \left((u_{s-1st} - R_s i_{s-1st})^2 + (u_{s-3rd} - R_s i_{s-3rd})^2 + (u_{s-5th} - R_s i_{s-5th})^2 \right) \quad (9)$$

Note that the values of R_s , u_{s-1st} , i_{s-1st} , u_{s-3rd} , i_{s-3rd} , u_{s-5th} and i_{s-5th} in (9) are obtained by averaging the corresponding values of the m stator phases. It is noted that voltages and currents in (9) are expressed in peak values.

The first harmonic component of the back electromotive force is calculated as,

$$e_{s-1st} = u_{s-1st} - i_{s-1st} \cdot R_s \quad (10)$$

Once the back electromotive force and the electrical angular velocity are known, the absolute value of the stator flux linkage can be determined as,

$$\psi_{s-1st} = e_{s-1st} / \omega_m \quad (11)$$

Fig. 7 shows the d - q electrical model.

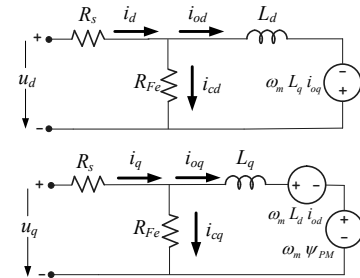


Fig. 7. d - q electrical model of the PMSM.

C. Differential voltage due to the current harmonics and angles determination

After performing the harmonic decomposition of the phase voltages and currents, the current and voltage phase angles for every component are obtained. Thus, the first harmonic power factor (average value of all m phases) can be calculated as,

$$\cos \phi = \frac{1}{m} \cdot \sum_{i=1}^m \cos(\theta_{u_{s-1st,i}} - \theta_{i_{s-1st,i}}) \quad (12)$$

$\theta_{u_{s-1st,i}}$ and $\theta_{i_{s-1st,i}}$ being, respectively, the angles of the voltage and current vectors of phase i .

Considering the harmonic contribution, the total power factor is calculated as,

$$\cos(\phi + \Delta\phi) = \frac{1}{m} \sum_{i=1}^m \frac{\text{mean}(u_i(t) \cdot i_i(t))}{U_{i-RMS} \cdot I_{i-RMS}} \quad (13)$$

The differential power factor angle $\Delta\phi$, which is required for an accurate calculation of the d - q inductances is calculated as,

$$\Delta\phi = \frac{1}{m} \sum_{i=1}^m (\theta_{u_{s,i}} - \theta_{i_{s-1st,d}}) \quad (14)$$

The angle between the first harmonic current space vector i_{s-1st} and the stator flux linkage Ψ_{s-1st} can be calculated in this stage. Fig. 8 shows the angles to be fixed during the identification process. It is noted that β is the angle between the first harmonic of the stator voltage and the back-electromotive force, ϕ the angle between the first harmonic of the stator current and voltage, and α the angle between the first harmonic of the stator flux linkage and current. By applying the sinus theorem, angle β is calculated as,

$$\sin\beta = \sin\phi \cdot \frac{i_{s-1st} \cdot R_s}{e_{s-1st}} \quad (15)$$

Thus, the angle between the first harmonic of the stator flux linkage and the current is,

$$\alpha = \frac{\pi}{2} - \beta - \phi \quad (16)$$

The definition of these angles helps to fix the relative position of all space vectors, allowing to have only one degree of freedom when finding the control angle, which in this case is the stator current angle, as detailed in the following subsections.

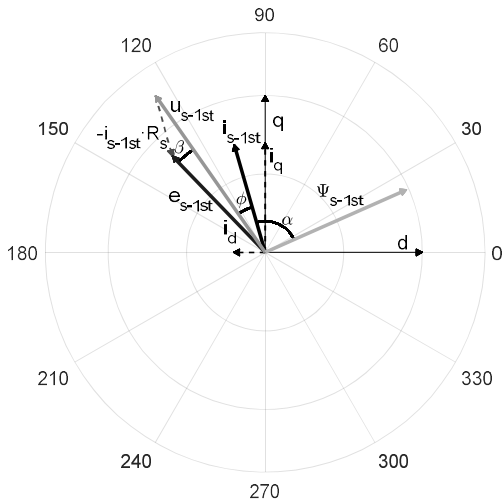


Fig. 8. PMSM d - q current, voltage and Ψ_{s-1st} Blondel diagram.

D. Inductance calculation and flux linkage, torque, voltage and power factor error

After discretizing the current space vector angle, the electrical magnitudes and errors of all discrete angles are obtained. First, the current space vector is decomposed in the d - q plane as,

$$\begin{cases} i_d = i_{s-1st} \cdot \cos(\theta_{i_{s-1st}}) \\ i_q = i_{s-1st} \cdot \sin(\theta_{i_{s-1st}}) \end{cases} \quad (17)$$

Next, as the angle between the stator flux linkage and the current is known, the stator flux linkage is obtained as follows,

$$\begin{cases} \psi_d = \psi_{s-1st} \cdot \cos(\theta_{i_{s-1st}} - \alpha) \\ \psi_q = \psi_{s-1st} \cdot \sin(\theta_{i_{s-1st}} - \alpha) \end{cases} \quad (18)$$

According to the literature [6], when calculating the inductance from the first harmonic components of the phase voltages and currents, when the current has a small value some issues occur, i.e., when the current angle is almost aligned with

the q -axis ($\theta_{is} \approx \pi/2$) or with the d -axis ($\theta_{is} \approx \pi$). Thus, an alternative way to calculate the d - q inductances is proposed, which considers the third and fifth harmonics of the current and the differential power factor angle $\Delta\phi$ (14).

- 1: Set the Current Angle Steps: $\theta_{i_{s-1st}} = \pi/2 : \Delta\theta_{i_{s-1st}} : \pi$
- 2: List the Operational Points: $P_{T_i} = \begin{bmatrix} T_{\min}, n_{\min} & \dots & T_{\min}, n_{\max} \\ \dots & \dots & \dots \\ T_{\max}, n_{\min} & \dots & T_{\max}, n_{\max} \end{bmatrix}$
- 3: **for** $P_{T_{\min}n_{\min}}$ to $P_{T_{\max}n_{\max}}$ **do**
- 4: FFT Electrical Magnitudes: $u_{s-1st,3rd,5th}, i_{s-1st,3rd,5th}, \cos(\phi)$
- 5: Winding Resistance Temperature Correction: R_s
- 6: Iron and Mechanical Losses: P_{Fe-mec}
- 7: Equivalent Iron-Mechanical Losses Resistance: R_{Fe-mec}
- 8: Back-Electromotive Force: e_{s-1st}
- 9: Stator Flux Linkage: ψ_{s-1st}
- 10: **for** $\theta_{i_{s-1st}} = \pi/2$ to $\theta_{i_{s-1st}} = \pi$ **do**
- 11: d - q Currents: $\begin{cases} i_d = i_{s-1st} \cdot \cos(\theta_{i_{s-1st}}) \\ i_q = i_{s-1st} \cdot \sin(\theta_{i_{s-1st}}) \end{cases}$
- 12: d - q Flux Linkages: $\begin{cases} \psi_d = \psi_{s-1st} \cdot \cos(\theta_{i_{s-1st}} - \alpha) \\ \psi_q = \psi_{s-1st} \cdot \sin(\theta_{i_{s-1st}} - \alpha) \end{cases}$
- 13: d - q Differential Voltages: $\begin{cases} \Delta u_d = |u_s| \cdot \cos(\theta_{i_{s-1st}} + \phi + \Delta\phi) - u_{s-1st} \cdot \cos(\theta_{i_{s-1st}} + \phi) \\ \Delta u_q = |u_s| \cdot \sin(\theta_{i_{s-1st}} + \phi + \Delta\phi) - u_{s-1st} \cdot \sin(\theta_{i_{s-1st}} + \phi) \end{cases}$
- 14: d - q Inductances: $\begin{cases} L_d = \frac{\Delta u_d + \Delta u_q}{|\Delta u_d|} \cdot 2 \cdot (3 \cdot \omega_m \cdot i_{s-3rd} + 5 \cdot \omega_m \cdot i_{s-5th}) \\ L_q = \frac{\Delta u_q - \Delta u_d}{|\Delta u_q|} \cdot 2 \cdot (3 \cdot \omega_m \cdot i_{s-3rd} + 5 \cdot \omega_m \cdot i_{s-5th}) \end{cases}$
- 15: Calculated d - q Flux Linkages: $\begin{cases} \psi_{d-calc} = \psi_{pm-1st} + L_d \cdot i_d \\ \psi_{q-calc} = L_q \cdot i_q \end{cases}$
- 16: d - q Flux Linkages errors: $\begin{cases} \varepsilon_{\psi_d} = (\psi_{d-calc} - \psi_d) / \psi_d \\ \varepsilon_{\psi_q} = (\psi_{q-calc} - \psi_q) / \psi_q \end{cases} \quad \varepsilon_{\psi_s} = \frac{1}{2} \cdot \varepsilon_{\psi_d} + \frac{1}{2} \cdot \varepsilon_{\psi_q}$
- 17: **end**
- 18: Minimum Flux Linkage error selection.
- 19: Calculated d - q Voltages: $\begin{cases} u_{d-calc} = R_s \cdot i_d - \omega_m \cdot \psi_q \\ u_{q-calc} = R_s \cdot i_q + \omega_m \cdot \psi_d \end{cases}$
 $u_{s-calc} = \sqrt{u_{d-calc}^2 + u_{q-calc}^2}$
- 20: Power Factor: $\cos\phi_{calc} = \cos(\theta_{u_{s-calc-1st}} - \theta_{i_{s-1st}})$
- 21: d - q Currents: $\begin{cases} i_{od} = i_d + \omega_m \cdot \psi_q / R_{Fe-mec} \\ i_{oq} = i_q - \omega_m \cdot \psi_d / R_{Fe-mec} \end{cases}$
- 22: Torque: $T = \left(\frac{m}{2}\right) \cdot p \cdot (\psi_d \cdot i_{oq} - \psi_q \cdot i_{od})$
- 23: Error: $\begin{cases} \varepsilon_T = \frac{|T - T_{ref}|}{T_{ref}} \\ \varepsilon_{u_s} = \frac{|u_{s-calc-1st} - u_{s-1st}|}{u_{s-1st}} \\ \varepsilon_{\cos(\rho)} = \frac{|\cos\phi_{calc} - \cos\phi|}{\cos\phi} \end{cases}$
- 24: **end**

Fig. 9. Sequence of the applied parameter estimation algorithm.

First, the differential d - q voltages due to the differential power factor angle are calculated as,

$$\begin{cases} \Delta u_d = |u_s| \cdot \cos(\theta_{i_{s-1st}} + \phi + \Delta\phi) - u_{s-1st} \cdot \cos(\theta_{i_{s-1st}} + \phi) \\ \Delta u_q = |u_s| \cdot \sin(\theta_{i_{s-1st}} + \phi + \Delta\phi) - u_{s-1st} \cdot \sin(\theta_{i_{s-1st}} + \phi) \end{cases} \quad (19)$$

Next, the inductances can be calculated as,

$$\begin{cases} L_d = \frac{\Delta u_q + \Delta u_d}{\frac{\Delta u_d}{|\Delta u_d|} \cdot 2 \cdot (3 \cdot \omega_m \cdot i_{s-3rd} + 5 \cdot \omega_m \cdot i_{s-5th})} \\ L_q = \frac{\Delta u_q - \Delta u_d}{\frac{\Delta u_q}{|\Delta u_q|} \cdot 2 \cdot (3 \cdot \omega_m \cdot i_{s-3rd} + 5 \cdot \omega_m \cdot i_{s-5th})} \end{cases} \quad (20)$$

Once the d - q inductances are known, the d - q flux linkages can be compared with those calculated using (18). Thus, for each discrete current angle, the relative error can be obtained.

$$\begin{cases} \psi_{d-calc} = \psi_{pm-1st} + L_d \cdot i_d \\ \psi_{q-calc} = L_q \cdot i_q \end{cases} \quad (21)$$

$$\begin{cases} \varepsilon_{\psi_d} = \frac{\psi_{d-calc} - \psi_d}{\psi_d} \\ \varepsilon_{\psi_q} = \frac{\psi_{q-calc} - \psi_q}{\psi_q} \end{cases} \quad \varepsilon_{\psi_s} = \frac{1}{2} \cdot \varepsilon_{\psi_d} + \frac{1}{2} \cdot \varepsilon_{\psi_q} \quad (22)$$

The space vector current angle $\theta_{i_{s-1st}}$ providing the minimum d - q flux linkage error is the nearest solution of the actual control angle. Once the optimal angle $\theta_{i_{s-1st}}$ is found, the values of the first harmonic components are calculated and compared with those extracted from the experimental data. The d - q voltages can be calculated taking into account the d - q current and flux linkage components.

$$\begin{cases} u_{d-calc} = R_s \cdot i_d - \omega_m \cdot \psi_q \\ u_{q-calc} = R_s \cdot i_q + \omega_m \cdot \psi_d \end{cases} \quad (23)$$

$$u_{s-calc} = \sqrt{u_{d-calc}^2 + u_{q-calc}^2} \quad (24)$$

The power factor can be calculated from the d - q voltages and the current vector as,

$$\cos(\phi_{calc}) = \cos(\theta_{u_{s-calc-1st}} - \theta_{i_{s-1st}}) \quad (25)$$

Considering the d - q electrical model, the torque generating currents, i_{od} and i_{oq} are calculated as,

$$\begin{cases} i_{od} = i_d + \frac{\omega_m \cdot \psi_q}{R_{Fe-mec}} \\ i_{oq} = i_q - \frac{\omega_m \cdot \psi_d}{R_{Fe-mec}} \end{cases} \quad (26)$$

Finally, the torque can be calculated as,

$$T = \left(\frac{m}{2}\right) \cdot p \cdot (\psi_d \cdot i_{oq} - \psi_q \cdot i_{od}) \quad (27)$$

Torque, voltage and power factor relative errors are calculated as,

$$\begin{cases} \varepsilon_T = \frac{|T - T_{ref}|}{T_{ref}} \\ \varepsilon_{u_s} = \frac{|u_{s-calc} - u_{s-1st}|}{u_{s-1st}} \\ \varepsilon_{\cos(\rho)} = \frac{|\cos \phi_{calc} - \cos \phi|}{\cos \phi} \end{cases} \quad (28)$$

Fig. 9 summarizes the parameter and FOC strategy identification algorithm. Once the entire combination of current and flux linkage angles has been analyzed, the specific combination matching with the PMSM operation is selected.

V. RESULTS

This section presents the results attained with the method developed in this work. First, the method is validated using an ABB PMSM driven by a DGV700 ABB converter, which is connected to a resolver, thus enabling to compare the control angle calculated by the model proposed in this paper with the experimental acquisitions. Next, the method proposed here is further validated by using a PMSM from Midtal Talentos driven by a RENESAS sensorless FOC control platform YROTATE-IT-RX23T with flux weakening capability. In this case, the current vector and the d - q inductance values provided by the model are compared against experimental data.

A. ABB PMSM

Table IV summarizes the relevant characteristics of the PMSM from ABB.

TABLE IV
ABB PMSM CHARACTERISTICS

Manufacturer	ABB
Converter model	DGV 700
Rated Voltage [V _{RMS}]	380
Rated Current [A _{RMS}]	2.9
Rated Torque [N·m]	2.3
Rated Speed [1/min]	6000

Fig. 10 compares in a Blondel diagram the values of the d - q currents provided by the parameter estimation model and the experimental values.

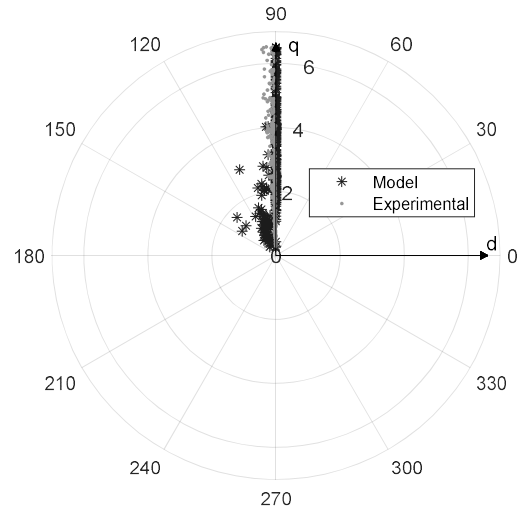


Fig. 10. ABB PMSM d - q Blondel current diagram.

According to Fig. 10, the model calculates correctly the control angle. The ABB PMSM drive applies a 90-degree current angle control without flux weakening capability.

B. GNC PMSM

In order to perform a deeper analysis of the method proposed in this work, a PMSM driven by a RENESAS sensorless FOC control platform YROTATE-IT-RX23T with flux weakening capability is studied. Table V summarizes the basic characteristics of the second PMSM, named GNC.

TABLE V
GNC PMSM CHARACTERISTICS

Manufacturer	Midal Talentos S.L
Converter model	RENESAS YROTATE-IT-RX32T
Rated Voltage [V _{RMS}]	200
Rated Current [A _{RMS}]	3
Rated Torque [N·m]	1
Rated Speed [1/min]	4600

Fig. 11 shows the d - q space vector current calculated by the parameter estimation algorithm in a Blondel diagram. It cannot be compared against experimental data because of the experimental sensorless strategy applied. As can be seen, most of the working points are in the quadrature axis, but when applying a flux weakening control some points move away from the quadrature axis.

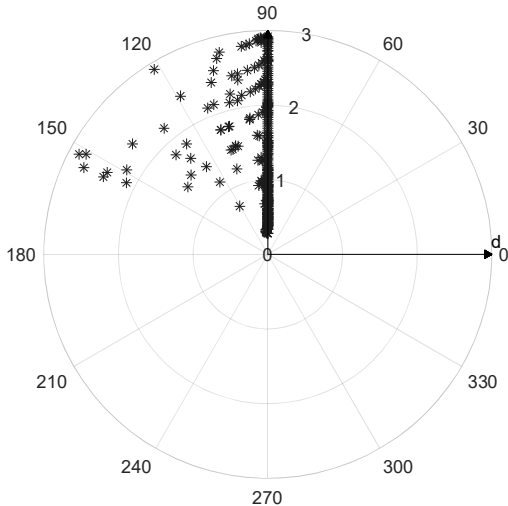


Fig. 11. GNC PMSM d - q Blondel current diagram.

C. Reference method for inductance measurement

The identified values of the inductance are compared against the values obtained with a reference experimental method described in [30], using a DC bias AC source. This method allows measuring the d - q inductances under different saturation conditions. To acquire the saturation effect, the AC signal peak value is set relatively small compared with the DC voltage bias. In this case the peak-to-peak voltage was set to 1 V, whereas the DC component was swept from 5 to 15 V, so the inductance can be expressed as a function of the DC voltage bias. This DC component represents the d - q voltage component of the model producing the corresponding the d - q current.

Fig. 12 shows the experimental setup used to measure the inductance by applying the reference experimental method.

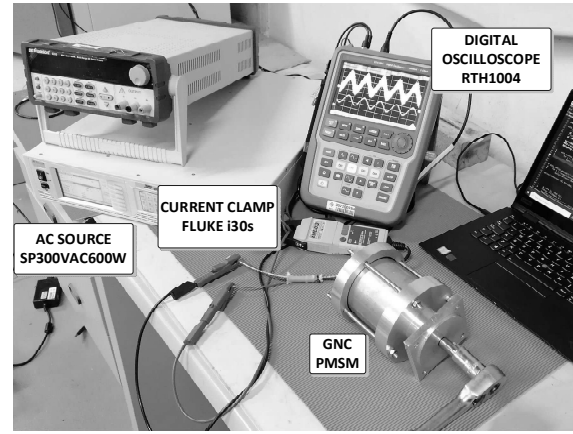


Fig. 12. Experimental setup to measure the d - q inductances calculation using an AC source allowing a DC bias.

Table VI summarizes the instrumentation used for the experimental validation of the inductance with the reference method.

TABLE VI
INDUCTANCE MEASUREMENT INSTRUMENTATION

AC Source	APM SP300VA600W ($I_{\max}=5.6$ A, $P_{\text{out}}=600$ W, 0.5 %)
Current Transducer	Fluke i30s (± 30 A, 100 mV/A, 1%)
Oscilloscope	ROHDE & SCHWARZ RTH1004 $\pm(0.05\%+0.03\%)$

Figs. 13 and 14 show the d - q inductance values for all current points depicted in Fig. 11. The identified values of the d - q inductances are compared point by point against the ground truth data obtained through the validated experimental method.

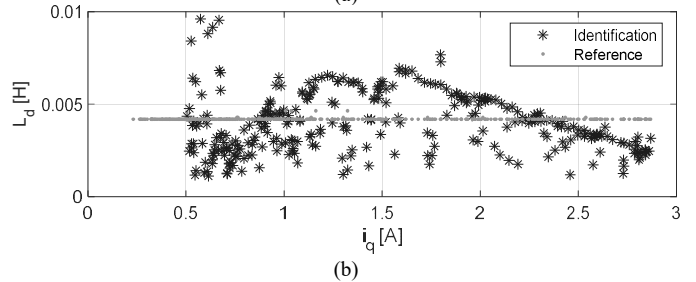
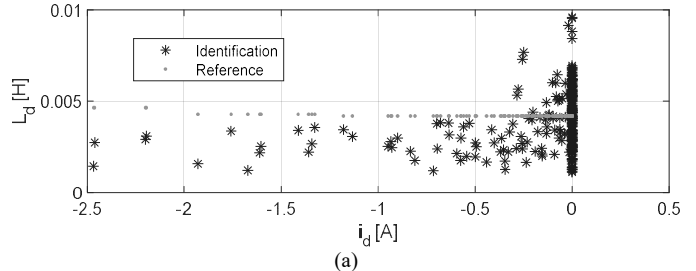
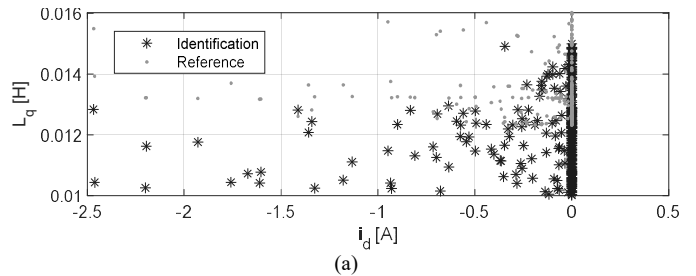


Fig. 13. Identified values of L_d versus the measured ones with the reference method. (a) L_d against i_d . (b) L_d against i_q .



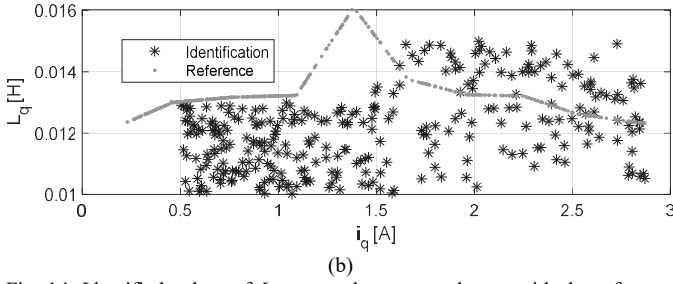


Fig. 14. Identified values of L_q versus the measured ones with the reference method. (a) L_q against i_d . (b) L_q against i_q .

As can be seen in Figs. 13 and 14, the model is able to identify accurately the magnitude of the d - q inductances.

The reference method averages the value of the inductance over one period of the current waveform, requiring to block the rotor during the tests, so the measured inductance values depend on the rotor position. However, the method proposed in this paper calculates the inductance for all considered working conditions when the machine operates under normal conditions. For this reason, from the scatter of points obtained by applying the proposed method, the mean value is obtained and compared with that of the reference method.

Table VII compares the reference values of the d - q inductances and the permanent magnet flux linkage with those identified by the method proposed in this paper.

TABLE VII
GNC PMSM. EXPERIMENTAL VERSUS MODEL PARAMETERS

Magnitudes	Identified values	Experimental
Direct inductance L_d [mH]	3.91 (mean value)	4.18
Quadrature inductance L_q [mH]	12.10 (mean value)	13.40
Permanent magnet flux linkage Ψ_{PM-1st} [V·s/rad]	0.080	0.083

D. Accuracy of the estimated parameters

This subsection determines the accuracy of the estimated parameters by using the combined standard uncertainty.

The combined standard variance of the d - q inductances (20) u_{c-Ld} and u_{c-Lq} is calculated as,

$$\begin{cases} u_{c-Ld}^2 = \left(\frac{\partial L_d}{\partial \Delta u_d} \right)^2 \cdot u^2(\Delta u_d) + \left(\frac{\partial L_d}{\partial \Delta u_q} \right)^2 \cdot u^2(\Delta u_q) + \left(\frac{\partial L_d}{\partial \omega_m} \right)^2 \cdot u^2(\omega_m) + \\ \left(\frac{\partial L_d}{\partial i_{s-3rd}} \right)^2 \cdot u^2(i_{s-3rd}) + \left(\frac{\partial L_d}{\partial i_{s-5th}} \right)^2 \cdot u^2(i_{s-5th}) \\ u_{c-Lq}^2 = \left(\frac{\partial L_q}{\partial \Delta u_d} \right)^2 \cdot u^2(\Delta u_d) + \left(\frac{\partial L_q}{\partial \Delta u_q} \right)^2 \cdot u^2(\Delta u_q) + \left(\frac{\partial L_q}{\partial \omega_m} \right)^2 \cdot u^2(\omega_m) + \\ \left(\frac{\partial L_q}{\partial i_{s-3rd}} \right)^2 \cdot u^2(i_{s-3rd}) + \left(\frac{\partial L_q}{\partial i_{s-5th}} \right)^2 \cdot u^2(i_{s-5th}) \end{cases} \quad (29)$$

As can be seen in (29) the d - q inductances are derived with respect to the d - q voltages, angular speed and the 3rd and 5th current harmonic components. The expressions result as,

$$\begin{aligned} u_{c-Ld}^2 &= \left(\frac{1/2}{\omega_m \cdot (3 \cdot i_{s-3rd} + 5 \cdot i_{s-5th})} \right)^2 \cdot u^2(\Delta u_d) + \\ &\left(\frac{1/2}{\omega_m \cdot (3 \cdot i_{s-3rd} + 5 \cdot i_{s-5th})} \right)^2 \cdot u^2(\Delta u_q) + \left(\frac{-(\Delta u_q + \Delta u_d) \cdot 1/2}{(3 \cdot i_{s-3rd} + 5 \cdot i_{s-5th}) \cdot \omega_m^2} \right)^2 \cdot u^2(\omega_m) + \\ &\left(\frac{-(\Delta u_q + \Delta u_d) \cdot 3/2}{\omega_m \cdot (3 \cdot i_{s-3rd} + 5 \cdot i_{s-5th})} \right)^2 \cdot u^2(i_{s-3rd}) + \left(\frac{-(\Delta u_q + \Delta u_d) \cdot 5/2}{\omega_m \cdot (3 \cdot i_{s-3rd} + 5 \cdot i_{s-5th})} \right)^2 \cdot u^2(i_{s-5th}) \end{aligned} \quad (30)$$

$$\begin{aligned} u_{c-Lq}^2 &= \left(\frac{1/2}{\omega_m \cdot (3 \cdot i_{s-3rd} + 5 \cdot i_{s-5th})} \right)^2 \cdot u^2(\Delta u_d) + \\ &\left(\frac{-1/2}{\omega_m \cdot (3 \cdot i_{s-3rd} + 5 \cdot i_{s-5th})} \right)^2 \cdot u^2(\Delta u_q) + \left(\frac{-(\Delta u_q - \Delta u_d) \cdot 1/2}{(3 \cdot i_{s-3rd} + 5 \cdot i_{s-5th}) \cdot \omega_m^2} \right)^2 \cdot u^2(\omega_m) + \\ &\left(\frac{-(\Delta u_q - \Delta u_d) \cdot 3/2}{\omega_m \cdot (3 \cdot i_{s-3rd} + 5 \cdot i_{s-5th})} \right)^2 \cdot u^2(i_{s-3rd}) + \left(\frac{-(\Delta u_q - \Delta u_d) \cdot 5/2}{\omega_m \cdot (3 \cdot i_{s-3rd} + 5 \cdot i_{s-5th})} \right)^2 \cdot u^2(i_{s-5th}) \end{aligned} \quad (31)$$

The $u^2(\Delta u_d)$, $u^2(\Delta u_q)$, $u^2(\omega_m)$, $u^2(i_{s-3rd})$ and $u^2(i_{s-5th})$ terms are substituted by the values summarized in Table III. The standard variance of the electrical angular speed, $u^2(\omega_m)$, is directly obtained from the fundamental frequency of the electrical currents calculated by means of the FFT, which has an accuracy of 1.0 Hz. The standard uncertainty of each parameter is obtained by applying the square root of (30) and (31), whereas the accuracy is calculated as the standard uncertainty multiplied by a coverage factor of 3 to ensure a 99% confidence level.

In (30)-(31) the current harmonic components are dividing, so for low currents, the third and fifth harmonic components have a large contribution in the combined variance, this contribution being more important at low speed operation.

Fig. 15 and Fig. 16 show the accuracy of the d - q inductances for all analyzed operating points.

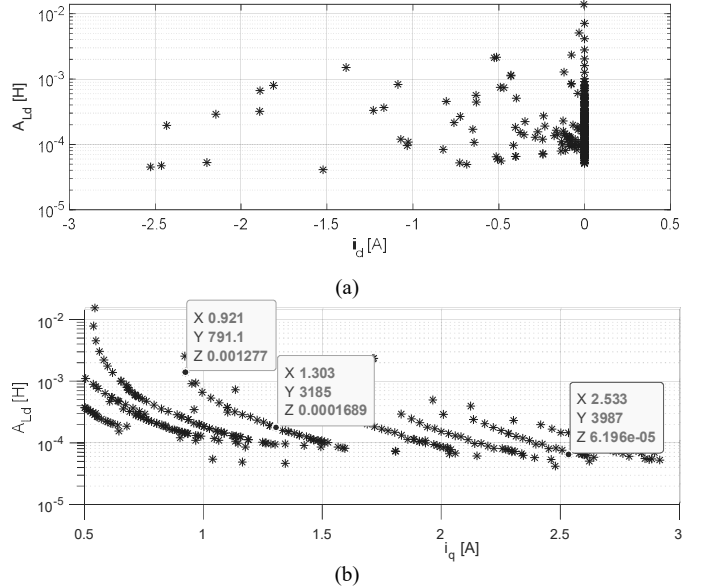
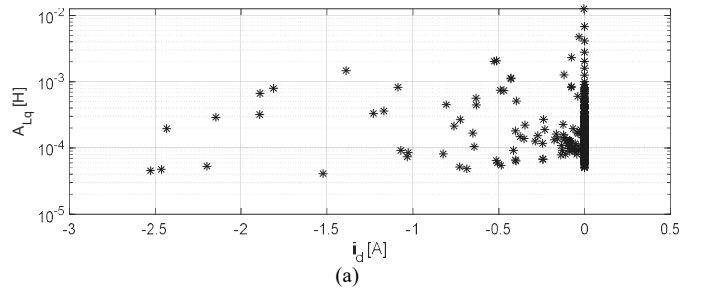


Fig. 15. Accuracy of the identified values of L_d (A_{Ld}) versus the accuracy of the measured ones with the reference method. (a) A_{Ld} versus i_d . (b) A_{Ld} versus i_q .



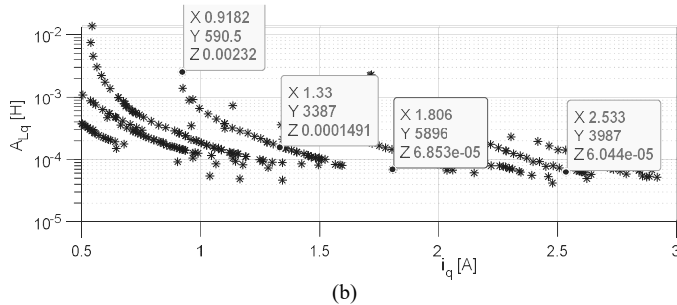


Fig. 16. Accuracy of the identified values of L_q (A_{Lq}) versus the accuracy of the measured ones with the reference method. (a) A_{Lq} versus i_d . (b) A_{Lq} versus i_q .

As can be observed, the accuracy is poorer at low currents and low angular speeds. For instance, the labels in Fig. 15 (b) and Fig. 16 (b) show that the accuracy increases with the angular speed (Y values of data labels).

Table VIII shows the mean accuracy of the estimated d - q inductances by applying (30)-(31). The accuracy is calculated with a coverage factor of 3, ensuring a confidence level of 99%.

TABLE VIII
GNC PMSM PARAMETER ESTIMATION ACCURACY

Magnitudes	Absolute accuracy [mH]
Direct inductance accuracy A_{Ld} [mH]	0.56 mH (mean value)
Quadrature inductance accuracy A_{Lq} [mH]	0.56 mH (mean value)

E. Computational burden

For both cases analyzed, the proposed parameter estimation method requires 0.66 seconds to calculate all points displayed in Figs. 12 and 13 using an Intel® Core™ i9-7940X 3.10 GHz processor with 64 GB RAM memory.

VI. CONCLUSIONS

This paper has presented a new method to estimate the PMSM electromagnetic parameters. The method allows characterizing the motor parameters by considering its performance on the entire torque-speed range, thus, allowing to find the parameter variations as a function of the load conditions. As a main novelty, the identification of the d - q inductances is based on the differential power factor due to the harmonic distortion. To identify the vectors magnitudes and angles, the method does not require any geometry information, no prior knowledge of the control strategy and does not need any position sensor. The method is based on a d - q electrical model with harmonic decomposition without requiring any optimization algorithm to identify the parameters, thus reducing the computational burden. As the main objective is to identify the parameters in the whole torque-speed range, the method can be classified as off-line. However, it can be applied on-line as well as for identifying the electromagnetic parameters from a unique operating point. The algorithm was validated using two PMSMs. Results presented show an accurate identification of the current space vector and the d - q inductances. The estimation is performed in an affordable time.

VII. REFERENCES

[1] Z. H. Liu, H. L. Wei, X. H. Li, K. Liu, and Q. C. Zhong, "Global Identification of Electrical and Mechanical Parameters in PMSM Drive Based on Dynamic Self-Learning PSO," *IEEE Trans. Power Electron.*, vol. 33, no. 12, pp. 10858–10871, Dec. 2018, doi: 10.1109/TPEL.2018.2801331.

[2] J. Pyrhonen, T. Jokinen, and V. Hrabovcová, *Design of rotating electrical machines*, 2nd edn. Hoboken: Wiley, 2013.

[3] O. Sandre-Hernandez, R. Morales-Caporal, J. Rangel-Magdaleno, H. Peregrina-Barreto, and J. N. Hernandez-Perez, "Parameter Identification of PMSMs Using Experimental Measurements and a PSO Algorithm," *IEEE Trans. Instrum. Meas.*, vol. 64, no. 8, pp. 2146–2154, Aug. 2015, doi: 10.1109/TIM.2015.2390958.

[4] N. Bianchi, *Electrical Machine Analysis Using Finite Elements*. CRC Press, 2005.

[5] K. Liu, J. Feng, S. Guo, L. Xiao, and Z. Q. Zhu, "Identification of flux linkage map of permanent magnet synchronous machines under uncertain circuit resistance and inverter nonlinearity," *IEEE Trans. Ind. Informatics*, vol. 14, no. 2, pp. 556–568, Feb. 2018, doi: 10.1109/TII.2017.2722470.

[6] M. S. Rafaq and J. W. Jung, "A Comprehensive Review of State-of-the-Art Parameter Estimation Techniques for Permanent Magnet Synchronous Motors in Wide Speed Range," *IEEE Trans. Ind. Informatics*, vol. 16, no. 7, pp. 4747–4758, Jul. 2020, doi: 10.1109/TII.2019.2944413.

[7] E. Armando, R. I. Bojoi, P. Guglielmi, G. Pellegrino, and M. Pastorelli, "Experimental identification of the magnetic model of synchronous machines," *IEEE Trans. Ind. Appl.*, vol. 49, no. 5, pp. 2116–2125, 2013, doi: 10.1109/TIA.2013.2258876.

[8] G. Pellegrino, B. Boazzo, and T. M. Jahns, "Magnetic Model Self-Identification for PM Synchronous Machine Drives," *IEEE Trans. Ind. Appl.*, vol. 51, no. 3, pp. 2246–2254, May 2015, doi: 10.1109/TIA.2014.2365627.

[9] S. A. Odhano, R. Bojoi, S. G. Roşu, and A. Tenconi, "Identification of the Magnetic Model of Permanent-Magnet Synchronous Machines Using DC-Biased Low-Frequency AC Signal Injection," *IEEE Trans. Ind. Appl.*, vol. 51, no. 4, pp. 3208–3215, Jul. 2015, doi: 10.1109/TIA.2015.2413383.

[10] A. Hosfeld, F. Hiester, and U. Konigorski, "Analysis of DC Motor Current Waveforms Affecting the Accuracy of 'Sensorless' Angle Measurement," *IEEE Trans. Instrum. Meas.*, vol. 70, 2021, doi: 10.1109/TIM.2020.3034598.

[11] J. Kim and J. S. Lai, "Quad Sampling Incremental Inductance Measurement through Current Loop for Switched Reluctance Motor," *IEEE Trans. Instrum. Meas.*, vol. 69, no. 7, pp. 4251–4257, Jul. 2020, doi: 10.1109/TIM.2019.2949319.

[12] G. Feng, C. Lai, K. Mukherjee, and N. C. Kar, "Current Injection-Based Online Parameter and VSI Nonlinearity Estimation for PMSM Drives Using Current and Voltage DC Components," *IEEE Trans. Transp. Electrification*, vol. 2, no. 2, pp. 119–128, Jun. 2016, doi: 10.1109/TTE.2016.2538180.

[13] M. S. Rafaq, F. Mwasilu, J. Kim, H. H. Choi, and J. W. Jung, "Online Parameter Identification for Model-Based Sensorless Control of Interior Permanent Magnet Synchronous Machine," *IEEE Trans. Power Electron.*, vol. 32, no. 6, pp. 4631–4643, Jun. 2017, doi: 10.1109/TPEL.2016.2598731.

[14] O. C. Kivanc and S. B. Ozturk, "Sensorless PMSM Drive Based on Stator Feedforward Voltage Estimation Improved with MRAS Multiparameter Estimation," *IEEE/ASME Trans. Mechatronics*, vol. 23, no. 3, pp. 1326–1337, Jun. 2018, doi: 10.1109/TMECH.2018.2817246.

[15] R. Raja, T. Sebastian, and M. Wang, "Online stator inductance estimation for permanent magnet motors using PWM excitation," *IEEE Trans. Transp. Electrification*, vol. 5, no. 1, pp. 107–117, Mar. 2019, doi: 10.1109/TTE.2019.2891047.

[16] D. Liang, J. Li, R. Qu, and W. Kong, "Adaptive second-order sliding-mode observer for PMSM sensorless control considering VSI Nonlinearity," *IEEE Trans. Power Electron.*, vol. 33, no. 10, pp. 8994–9004, Oct. 2018, doi: 10.1109/TPEL.2017.2783920.

[17] Y. Yan, J. Yang, Z. Sun, C. Zhang, S. Li, and H. Yu, "Robust Speed Regulation for PMSM Servo System with Multiple Sources of Disturbances via an Augmented Disturbance Observer," *IEEE/ASME Trans. Mechatronics*, vol. 23, no. 2, pp. 769–780, Apr. 2018, doi: 10.1109/TMECH.2018.2799326.

[18] W. Lu, B. Tang, K. Ji, K. Lu, D. Wang, and Z. Yu, "A New Load Adaptive Identification Method Based on an Improved Sliding Mode Observer for PMSM Position Servo System," *IEEE Trans. Power Electron.*, vol. 36, no. 3, pp. 3211–3223, Mar. 2021, doi: 10.1109/TPEL.2020.3016713.

[19] O. Wallscheid and J. Böcker, "Global identification of a low-order

lumped-parameter thermal network for permanent magnet synchronous motors,” *IEEE Trans. Energy Convers.*, vol. 31, no. 1, pp. 354–365, Mar. 2016, doi: 10.1109/TEC.2015.2473673.

- [20] W. Deng, C. Xia, Y. Yan, Q. Geng, and T. Shi, “Online Multiparameter Identification of Surface-Mounted PMSM Considering Inverter Disturbance Voltage,” *IEEE Trans. Energy Convers.*, vol. 32, no. 1, pp. 202–212, Mar. 2017, doi: 10.1109/TEC.2016.2621130.
- [21] L. Colombo, M. L. Corradini, A. Cristofaro, G. Ippoliti, and G. Orlando, “An Embedded Strategy for Online Identification of PMSM Parameters and Sensorless Control,” *IEEE Trans. Control Syst. Technol.*, vol. 27, no. 6, pp. 2444–2452, Nov. 2019, doi: 10.1109/TCST.2018.2862415.
- [22] C. Wu, Y. Zhao, and M. Sun, “Enhancing Low-Speed Sensorless Control of PMSM Using Phase Voltage Measurements and Online Multiple Parameter Identification,” *IEEE Trans. Power Electron.*, vol. 35, no. 10, pp. 10700–10710, Oct. 2020, doi: 10.1109/TPEL.2020.2978200.
- [23] M. Pulvirenti, G. Scarcella, G. Scelba, A. Testa, and M. M. Harbaugh, “On-line stator resistance and permanent magnet flux linkage identification on open-end winding PMSM Drives,” in *IEEE Transactions on Industry Applications*, Jan. 2019, vol. 55, no. 1, pp. 504–515, doi: 10.1109/TIA.2018.2869877.
- [24] H. Wang, K. Lu, D. Wang, and F. Blaabjerg, “Online Identification of Intrinsic Load Current Dependent Position Estimation Error for Sensorless PMSM Drives,” *IEEE Access*, vol. 8, pp. 163186–163196, Aug. 2020, doi: 10.1109/access.2020.3019690.
- [25] Q. Wang, G. Wang, N. Zhao, G. Zhang, Q. Cui, and D. Xu, “An Impedance Model-Based Multiparameter Identification Method of PMSM for Both Offline and Online Conditions,” *IEEE Trans. Power Electron.*, vol. 36, no. 1, pp. 727–738, Jan. 2021, doi: 10.1109/TPEL.2020.3000896.
- [26] A. Belqorchi, U. Karaagac, J. Mahseredjian, and I. Kamwa, “Standstill Frequency Response Test and Validation of a Large Hydrogenerator,” *IEEE Trans. Power Syst.*, vol. 34, no. 3, pp. 2261–2269, May 2019, doi: 10.1109/TPWRS.2018.2889510.
- [27] Q. Wang, G. Zhang, G. Wang, C. Li, and D. Xu, “Offline Parameter Self-Learning Method for General-Purpose PMSM Drives with Estimation Error Compensation,” *IEEE Trans. Power Electron.*, vol. 34, no. 11, pp. 11103–11115, Nov. 2019, doi: 10.1109/TPEL.2019.2900559.
- [28] X. Wu, X. Fu, M. Lin, and L. Jia, “Offline Inductance Identification of IPMSM with Sequence-Pulse Injection,” *IEEE Trans. Ind. Informatics*, vol. 15, no. 11, pp. 6127–6135, Nov. 2019, doi: 10.1109/TII.2019.2932796.
- [29] N. Leboeuf, T. Boileau, B. Nahid-Mobarakeh, N. Takorabet, F. Meibody-Tabar, and G. Clerc, “Estimating permanent-magnet motor parameters under inter-tum fault conditions,” in *IEEE Transactions on Magnetics*, Feb. 2012, vol. 48, no. 2, pp. 963–966, doi: 10.1109/TMAG.2011.2177642.
- [30] J. Nakatsugawa, Y. Notohara, D. Li, and Y. Iwaji, “Inductance measurement method for permanent magnet synchronous motors using AC with DC bias,” 2008, doi: 10.1109/ICELMACH.2008.4800054.



Antonio Garcia received the M.S. degree in electrical engineering and the Ph.D. degree from the Universitat Politècnica de Catalunya, in 2000 and 2005, respectively. He is with the Motion and Industrial Control Research Group (MCIA). His research interests include electromagnetic devices, electric machines, variable-speed drive systems, and fault-detection algorithms.

VIII. BIOGRAPHIES



Carlos Candelo-Zuluaga received the M.S. in industrial engineering from the Universitat Politècnica de Catalunya, Barcelona, Spain. Where he is currently working toward the Ph.D. degree in electrical engineering. His research interest includes the design and optimization of permanent magnet synchronous motors.



Jordi-Roger Riba (M’09) was born in Igualada, Spain, in 1966. He received the M.S. and Ph.D. degrees in physics from the Universitat de Barcelona, Barcelona, Spain, in 1990 and 2000, respectively. In 1992, he joined the Universitat Politècnica de Catalunya, where he is currently a Full professor. He is currently with the Motion Control and Industrial Applications Research Group (MCIA). His current research interests include modeling and simulation of electromagnetic devices, electrical machines and high-voltage engineering.